Coupling Extraction and Maximum Efficiency Tracking for Multiple Concurrent Transmitters in Dynamic Wireless Charging

Do-Hyeon Kim, Seongmin Kim, Sang-Won Kim, Jungick Moon, Inkui Cho, and Dukju Ahn

***Abstract*—We propose a fast maximum efficiency tracking, which instantly optimizes all. TX coils' currents using runtime-extracted mutual inductances, for simultaneously activated multiple TXs whose output levels are different each other. For fast control, we propose a theory to runtime extract all the mutual inductances between multiple TXs and an RX. Here, one prerequisite of extracting the values of mutual inductances is to acquire its relative ratios between the mutual inductances. It is proposed that the relative ratio can be obtained by reflected resistances and coil currents of each TX, which are ac quantities but can easily be measured using dc input property of *LCC* inverter. Using the ratio information in conjunction with RX dc output, the exact values of mutual inductances can be extracted. The aim of the proposed method is to enable fast (no iteration) maximum efficiency tracking for multiple TXs, which entails the optimization of the relative ratios among TX currents, as well as the RX load optimization. A 200-W RX moves at 10 km/h, and the controller can track the optimum target TX currents in response to time-varying magnetic couplings**

***Index Terms*—Dynamic charging, inductive power transfer, maximum efficiency point tracking (MEPT), wireless power transfer.**

I. Introduction

DYNAMIC wireless power transfer allows the receiver to move on the array of transmitter coils while seamless charging is not interrupted. One of the viable applications is wireless charging of automated guided vehicle (AGV) that moves along the designated track in factory or warehouse. By installing wireless charger on the track floor, the AGV can be runtime charged at 24 h without parking and stopping for manual charging. [1]–[7].

Manuscript received July 29, 2019; revised November 8, 2019; accepted December 18, 2019. Date of publication December 24, 2019; date of current version April 22, 2020. This work was supported by Electronics and Telecommunications Research Institute (ETRI) grant funded by the Korean government under Grant 1711078386(19ZR1240), under the Project Development of Intelligent Radio Wave Sensor and Wireless Power Transfer Technology. Recommended for publication by Associate Editor M. Duffy. *(Corresponding author: Dukju Ahn.)*

D.-H. Kim is with the Samsung Electronics, Suwon 16522, South Korea (e-mail: dndmoriah@gmail.com).

S. Kim, S.-W. Kim, J. Moon, and I. Cho are with the Electronics and Telecommunications Research Institute, Daejeon 34129, South Korea (e-mail: smkim97@etri.re.kr; melanio@etri.re.kr; jungick@etri.re.kr; cho303@etri.re.kr).

D. Ahn is with the Incheon National University, Incheon 22012, South Korea (e-mail: adjj22@gmail.com).

Color versions of one or more of the figures in this article are available online at http://ieeexplore.ieee.org.

Digital Object Identifier 10.1109/TPEL.2019.2962203

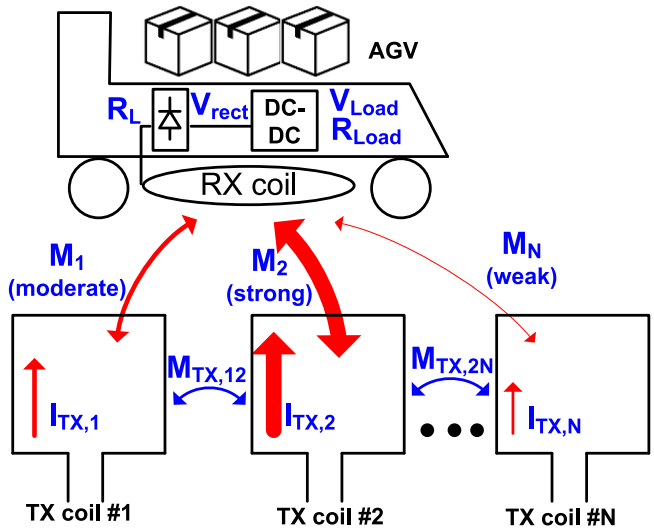

Fig. 1. Two requirements for maximum efficiency tracking for multiple TXs. The first requirement is the traditional optimum load impedance matching. The second requirement is to adjust the ratio between TX coil currents to be equal to the ratio between magnetic coupling, $I_{TX,1} : I_{TX,2} : I_{TX,N} = M_1 : M_2 : M_N$.

Meanwhile, maximum efficiency point tracking (MEPT) is an important research area of wireless power transfer community [8]–[17]. It adjusts its TX coil current output such that the impedance presented to RX coil is transformed to optimum load resistance, which maximizes overall efficiency. The MEPT enables the maximum possible efficiency for given parasitic and coupling parameters of coils because the overall efficiency is greatly affected by load impedance of RX coil.

Unfortunately, the MEPT technique is not well established for multiple-transmitter dynamic charging environment due to following reasons. Figs. 1 and 2 illustrate the requirements of maximum efficiency tracking for multiple-TX system. In addition to load impedance optimization of traditional single-TX MEPT, multiple-TX coils should be simultaneously activated with the relative ratio between TX coil currents being equal to the relative ratio between mutual inductances, as discussed in [18]–[20]. These are regarded as truly maximum efficiency point for multiple-TX environment. Another requirement is fast tracking speed in order to accommodate moving object, which becomes more complicated in multiple-activated-TX

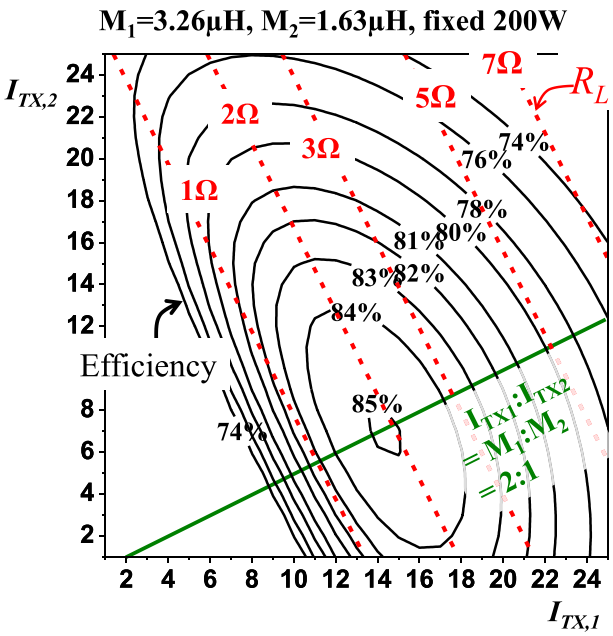

Fig. 2. Efficiency and load impedance versus $I_{TX,1}$ and $I_{TX,2}$ when M_1:M_2 = 2:1. Solid black contour is efficiency and red dotted contour is R_L that are resulted from $I_{TX,1}$ and $I_{TX,2}$. Solid green line is the set of $(I_{TX,1}, I_{TX,2})$ coordinates, where the current ratio matches the mutual inductance ratio. Maximum efficiency tracking for multiple transmitters requires the optimizations of both the current ratio and R_L. Parasitic resistance of coils is 0.15 Ω and fixed output of 200 W.

environment because the system needs to track the ratio of mutual inductances as well as the traditional optimum load impedance.

The optimum load tracking developed so far can be classified into a few categories. The most widespread is perturb and observe (P&O) tracking. This perturbs the effective load impedance seen by RX coil into higher (lower) value and observes the variation of efficiency. If the efficiency is increased, then the controller further increases (reduces) the effective load impedance [14]–[16]. This method is simple and robust. However, its tracking speed is rather slow because it is based on iteration process. The methods presented in [15] and [16] took a few seconds for the controller to converge to the optimum point. The method presented in [17] performs P&O for multiple transmitters at the speed of several hundred milliseconds.

One of the solutions to address the low-speed issue is linear control [11] for series resonant inverter with exact *LC* tuning at switching frequency. It is discussed that the voltage transfer gain from inverter input to receiver output has a certain value if the system is at maximum efficiency point. If there is deviation from maximum efficiency point, an error signal is developed. The controller detects this error signal and performs PI control such that the error is removed. Since this method does not iterate over operating status, it is faster than the P&O method. However, Huang *et al*. [11] cannot be applied to *LCC* inverter because the voltage transfer gain from *LCC* inverter to receiver output is not affected by the load impedance variations. In other words, the error signal is not generated in *LCC* inverter even if the load impedance is deviated from optimum. This is due to the fact that the TX coil current of *LCC* inverter is constant regardless of load. Similar problem exists for series *LC* inverter where the resonant frequency of *LC* is designed to be detuned from switching frequency. This method still shows 300-ms delay.

Another method of MEPT is to extract a mutual inductance between TX and RX coils. If coupling parameter is known, the MEPT can be performed fast. To this end, various methods of estimating the mutual inductance have been investigated. The methods presented in [21] and [22] sense impedance and voltage and proved that accurate estimation is possible. The method presented in [23] observes the transient waveform of TX coil current to estimate mutual inductance. This method does not require the information on receiver-side property. However, it should directly sense the resonant coil current and analyze the envelope variations of TX resonant current. This is complex, and the runtime implementation of this scheme is in fact not demonstrated. The method presented in [9] estimates the time-varying coupling coefficient in two steps. First step estimates initial coupling using the information on receiver output voltage and transmitter input. Second step estimates the latest coupling coefficient by observing the variation of duty cycle of TX-side dc–dc converter. This is simple in terms of sensing because the resonant currents of coils are not measured, instead the dc voltages and the duty cycle information of dc–dc converter are sufficient for control. Unfortunately, it took 100 ms for coupling estimation and additional 500 ms for converging to maximum efficiency point.

Among the various MEPT and coupling estimation methods discussed above, very few can actually be applicable to dynamic charging with multiple-activated-TX environment. Majority of them are developed for single-TX system except [17]—the optimization of relative ratio between TX currents is not considered, which is essential in achieving the truly maximum efficiency with multiple-TX coils, as shown in Fig. 1. In terms of speed, they took at least several hundreds of milliseconds to converge.

Coupling parameter extraction is useful for high-speed maximum efficiency tracking but extraction for multiple-activated TX coils has not been well studied. Simple extension of 1-TX estimation method into multiple-TX scenario is not feasible because there are ambiguities in the extracted couplings. In other words, suppose that there are two TX coils with mutual inductances of M_1 and M_2 and coil currents of $\mathbf{I_1}$ and $\mathbf{I_2}$, respectively. The RX open-circuit voltage $\mathbf{V_{OC}}$ is $\mathbf{V_{OC}} = j\omega M_1\mathbf{I_1} + j\omega M_2\mathbf{I_2}$. For a specific set of $\mathbf{V_{OC}}$ and TX coil currents, there exist many possible combinations of M_1 and M_2 that satisfy the abovementioned equation. The mutual inductances cannot be uniquely determined.

In this article, the M_1 and M_2 values are uniquely determined by finding another equation, which is the relative ratio between M_1 and M_2. We propose that the ratio of M_1 and M_2 can be extracted by multiplying the ratio of reflected resistance and the ratio of TX coil current. Although these are ac quantities, in the case of *LCC* inverter, these quantities can be inferred by dc input voltage and current of *LCC* inverter. Using the extracted mutual inductances, the controller not only optimizes the load impedance but also optimizes the relative strength ratio between TX coil currents (i.e., $I_{TX,1} : I_{TX,2} : I_{TX,N} = M_1 :$

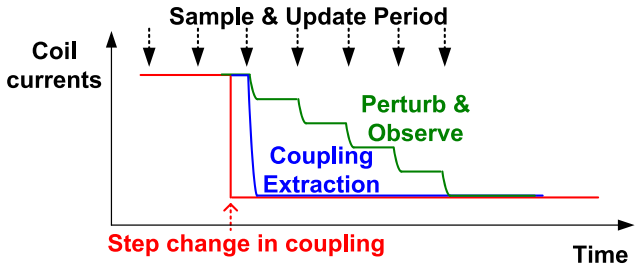

Fig. 3. Coupling coefficient extraction allows faster response than iterative methods.

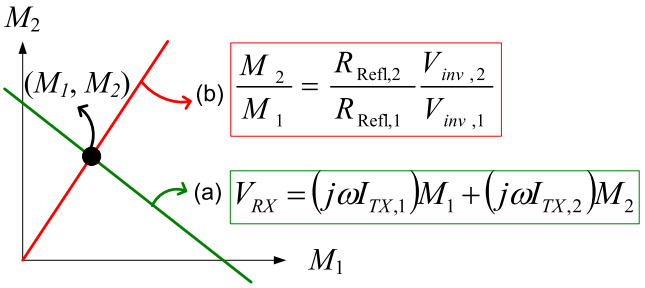

Fig. 4. (a) Combinations of M_1 and M_2, which are obtainable by the fundamental mutual inductance equation. For multiple transmitters, the mutual inductance equation cannot uniquely estimate the multiple mutual inductances. (b) Extracting the ratio between M_1 and M_2 is proposed in Section II-B, in order to uniquely determine an (M_1, M_2) point.

$M_2 : M_3$). The control is based on the runtime coupling extraction, hence obviates the necessity of perturbation and observe or iterations. This enables fast MEPT for multiple transmitters. The developed method is applied to automatic guided vehicle application for warehouse or factory at 10 km/h speed.

II. Runtime Extraction of TX–RX Coupling for Multiple Transmitters

A. Bottleneck of Mutual Inductance Extraction for Multiple-Transmitter System

Referring to Fig. 2, there are N-dimensional target variables $(I_{TX,1}, I_{TX,2}, \ldots, I_{TX,N})$ for system with number of N transmitters. This demands faster tracking methods. Coupling coefficient extraction allows faster tracking of maximum efficiency point than P&O, as shown in Fig. 3. The traditional coupling estimation methods are fundamentally based on mutual inductance equation, which relates the coil current of one side and resultant voltage induction at the other side such as $\mathbf{V_{RX}} = j\omega M \mathbf{I_{TX}}$ and $\mathbf{V_{TX}} = j\omega M \mathbf{I_{RX}}$ [22], [9].

Unfortunately, the expansion of this equation to concurrently active multi-TXs environment is not feasible. Fig. 4(a), green trace, represents the possible sets of M_1 and M_2 that satisfy the mutual inductance equation for two-transmitter example. The M_1 and M_2 cannot be uniquely determined. To resolve the ambiguity, Section II-B proposes that the relative ratio between M_1 and M_2 can be extracted using the TX-side voltage and impedances, as shown in Fig. 4(b), red trace. Using both traces of Fig. 4(a) and (b), the mutual inductances M_1 and M_2 can uniquely be extracted in Section II-C. The extracted M_1 and M_2 are to be used for maximum efficiency tracking in Section III.

B. Extracting the Ratios Between Mutual Inductances

The purpose of this section is to extract the $M_1 : M_2 : \ldots : M_k : \ldots : M_N$ ratio when simultaneously activated multiple TXs are present.

Fig. 5(a) presents the equivalent circuit. The ac input voltage into kth coil $L_{TX} - C_{TX}$, $\mathbf{V_k}$, is

$$\mathbf{V_k} = (R_{TX} + jX_{TX})\mathbf{I_{TX,k}} + j\omega \sum_{m=1, m\neq k}^{N} M_{TX,km}\mathbf{I_{TX,m}} + j\omega M_k \mathbf{I_{RX}} \quad (1)$$

where R_{TX} is the parasitic resistance of TX network, $X_{TX} = \omega L_{TX} - 1/(\omega C_{TX})$ is the reactive impedance of TX coil network, and $\mathbf{I_{TX,k}}$ and $\mathbf{I_{RX}}$ are the resonant current at kth TX coil and receiver, respectively. M_k is the mutual inductance between receiver and kth TX coil, whereas $M_{TX,km}$ is the coupling between kth TX coil and mth TX coil. Bold letters represent phasor notation that includes both real and imaginary part.

Dividing $\mathbf{V_k}$ with $\mathbf{I_{TX,k}}$ yields the total impedance at kth TX network, $\mathbf{Z_k}$, as

$$\mathbf{Z_k} = R_{TX} + jX_{TX} + j\omega \sum_{m=1, m\neq k}^{N} M_{TX,km} \frac{\mathbf{I_{TX,m}}}{\mathbf{I_{TX,k}}} + j\omega M_k \frac{\mathbf{I_{RX}}}{\mathbf{I_{TX,k}}}. \quad (2)$$

Here, the third term $j\omega \sum_{m=1, m\neq k}^{N} M_{TX,km}\mathbf{I_{TX,m}}/\mathbf{I_{TX,k}}$ is purely imaginary because all the $\mathbf{I_{TX,k}}$s are enforced to be in-phase to maximize the efficiency and output power, and hence $\mathbf{I_{TX,m}}/\mathbf{I_{TX,k}}$ is a real number. This is possible because *LCC* inverter has constant current characteristic, so the phase of $\mathbf{I_{TX,k}}$ is determined only by clock timing of switch bridge [18].

The last term

$$R_{\text{Refl},k} = j\omega M_k \frac{\mathbf{I_{RX}}}{\mathbf{I_{TX,k}}} \quad (3)$$

is the reflected resistance for each TX, which represents the actual power transfer from each TX to an RX. The receiver current $\mathbf{I_{RX}}$ is given as

$$\mathbf{I_{RX}} = -j\omega \frac{\sum_{m=1}^{N} M_m \mathbf{I_{TX,m}}}{R_{RX} + R_L}. \quad (4)$$

Hence, (3) becomes

$$R_{\text{Refl},k} = \frac{(\omega M_k)^2}{R_{RX} + R_L} + \frac{\omega^2 M_k}{R_{RX} + R_L} \frac{\sum_{m=1, m\neq k}^{N} M_m \mathbf{I_{TX,m}}}{\mathbf{I_{TX,k}}} \quad (5)$$

which is purely resistive.

Although the reflected resistance is an ac resistance and cannot be measured directly, there exists a relationship between inverter

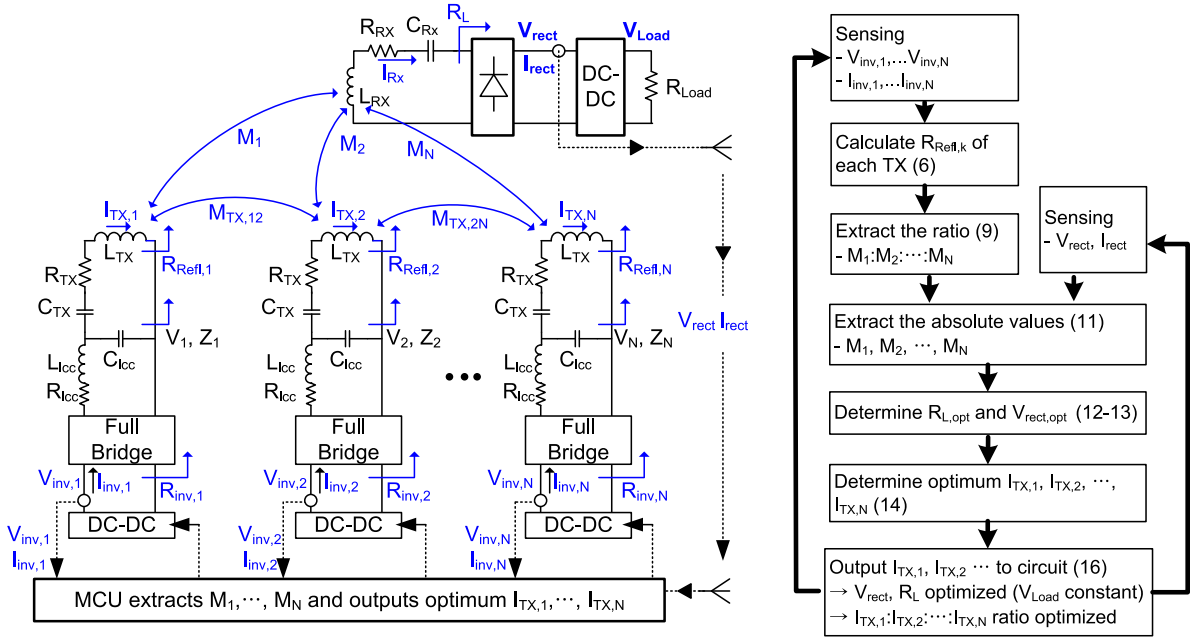

(a) (b)

Fig. 5. (a) Equivalent circuit of system. A global TX-side MCU extracts the M_1, M_2, ..., M_N using $V_{\mathrm{inv},k}$, $I_{\mathrm{inv},k}$, V_{rect}, and I_{rect}. This determines optimum $I_{TX,1}$, $I_{TX,2}$, ..., $I_{TX,N}$ that satisfies both the $I_{TX,1} : I_{TX,2} : I_{TX,N} = M_1 : M_2 : M_N$ and the $V_{\mathrm{rect}} = V_{\mathrm{rect.opt}}$. (b) Control flowchart. The scheme continuously monitors the dc voltage and currents, real-time calculates, and outputs the optimum TX currents. Optimum operating condition is achieved in one control cycle.

dc input resistance, $R_{\mathrm{inv},k}$, and reflected resistance such that

$$R_{\mathrm{Refl},k} = \frac{\pi^2}{8} \frac{1}{(\omega C_{\mathrm{lcc}})^2 (R_{\mathrm{inv},k} - R_{\mathrm{lcc}}\pi^2/8)} - R_{TX}. \quad (6)$$

Here, $R_{\mathrm{inv},k} = V_{\mathrm{inv},k}/I_{\mathrm{inv},k}$ is the ratio between dc input voltage and current of kth inverter, which can easily be measured. R_{lcc} is the parasitic resistance of L_{lcc}, which is 0.03 Ω in this article.

From (3), the ratio of reflected resistances between kth TX and jth TX is

$$\frac{R_{\mathrm{Refl},k}}{R_{\mathrm{Refl},j}} = \frac{M_k}{M_j} \frac{I_{TX,j}}{I_{TX,k}}. \quad (7)$$

Since $I_{TX} = (4/\pi)\omega C_{\mathrm{lcc}} V_{\mathrm{inv}}$ in *LCC* resonant inverter, (7) is rearranged as

$$\frac{M_k}{M_j} = \frac{R_{\mathrm{Refl},k}}{R_{\mathrm{Refl},j}} \frac{V_{\mathrm{inv},k}}{V_{\mathrm{inv},j}}. \quad (8)$$

Substituting (6) into (8) yields

$$\frac{M_k}{M_j} = \frac{\frac{\pi^2}{8(\omega C_{\mathrm{lcc}})^2 (R_{\mathrm{inv},k} - R_{\mathrm{lcc}}\pi^2/8)} - R_{TX}}{\frac{\pi^2}{8(\omega C_{\mathrm{lcc}})^2 (R_{\mathrm{inv},j} - R_{\mathrm{lcc}}\pi^2/8)} - R_{TX}} \frac{V_{\mathrm{inv},k}}{V_{\mathrm{inv},j}}. \quad (9)$$

In other words, the ratio of M_k and M_j can be runtime extracted by monitoring $V_{\mathrm{inv},k,j}$ and $R_{\mathrm{inv},k,j} = V_{\mathrm{inv},k,j}/I_{\mathrm{inv},k,j}$, which is the ratio of dc voltage and current and hence can easily be obtained by typical microcontrollers. The calculation of (9) uses the instantaneous dc voltage and current values, implying that fast acquisition and calculation is possible.

Equations (1)–(9) can also detect the negative polarity of mutual inductance M_k, which occurs when the receiver is significantly lateral misaligned from kth TX coil, and hence the RX is side-by-side from TX#k rather than vertically stacked on TX#k, as shown in Fig. 6. The magnitude of negative coupling is limited because negative coupling occurs when lateral misalignment is severe, as shown in Fig. 6. For negative M_k, the $R_{\mathrm{Refl},k}$ of (3) and $R_{\mathrm{inv},k}$ of (6) become also negative, and the direction of $I_{\mathrm{inv},k}$ is reversed. In fact, the controller deactivates TXs whose mutual inductance is significantly lower than other TXs. Hence, the negatively coupled TXs are deactivated, and their effect on performance is negligible.

Equation (9) is important for two reasons. Equation (9) provides the desired ratios to which the TX coil currents are matched, as shown in Fig. 1. Moreover, (9) is needed to extract the value of mutual inductances, which is presented in the following section.

C. Extracting Absolute Value of Mutual Inductances for Multiple Transmitters

To extract a value of mutual inductance M_k, the receiver rectifier output voltage V_{rect} is written as

$$V_{\mathrm{rect}} = \frac{(\pi/4)R_L}{R_{RX} + R_L} \omega \left| M_1 \mathbf{I_{TX,1}} + M_2 \mathbf{I_{TX,2}} + , \ldots , + M_N \mathbf{I_{TX,N}} \right|. \quad (10)$$

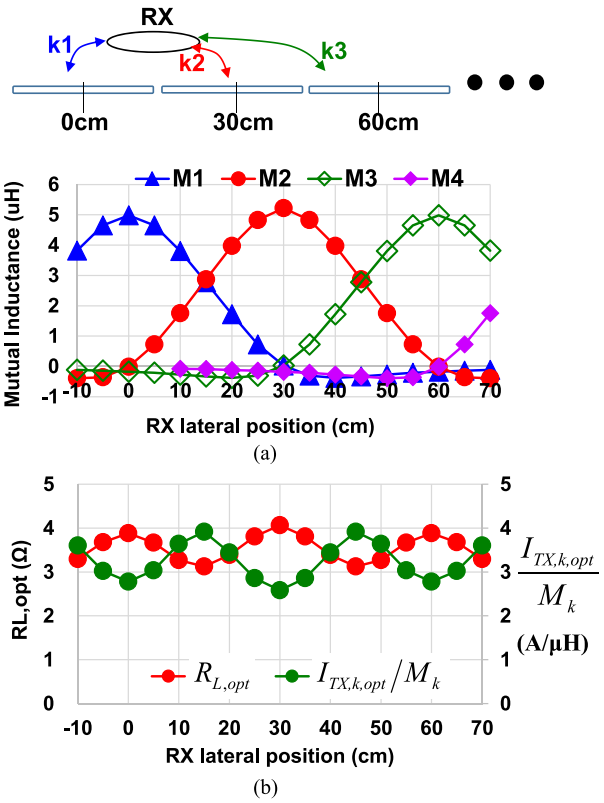

Fig. 6. RX lateral position is swept across TX area. The same characteristic repeats periodically. (a) Negative coupling when RX is lateral from TX. (b) Optimum load RL, opt for different sets of mutual inductances. Also illustrated is optimum proportionality factor $I_{TX,k,\mathrm{opt}}/M_k$ specified by (15).

There are many sets of $\{M_1, M_2, \ldots M_N\}$ that satisfy (10) for given V_{rect}, $\mathbf{I_{TX,1}}$, $\mathbf{I_{TX,2}}$, … $\mathbf{I_{TX,N}}$ values. However, dividing both sides of (10) by M_k and rearranging gives a unique value of M_k as follows:

$$M_k = \left(1 + \frac{R_{RX}}{R_L}\right) \frac{V_{\mathrm{rect}}}{\omega^2 C_{\mathrm{lcc}} \left(V_{\mathrm{inv},k} + \sum_{m=1,m\neq k}^{N} \frac{M_m}{M_k} V_{\mathrm{inv},m}\right)} \tag{11}$$

where the ratio M_m/M_k can be obtained by (9). The V_{rect} as well as $V_{\mathrm{inv},k}$ is also a dc quantity that is easily monitored. The $R_L = (8/\pi^2)V_{\mathrm{rect}}/I_{\mathrm{rect}}$ is extracted at the output of rectifier by dc voltage and current measurement.

Equation (11) states that unlike single-TX case, it is a prerequisite to know the ratios M_m/M_k in order to extract the M_k value in multiple-transmitter application.

III. $I_{\mathrm{TX,k}}$ Tracking to Satisfy Both the Optimum Load and Current Ratio

Referring to Fig. 2, the maximum efficiency tracking for multiple-transmitter dynamic charging should be able to identify both the optimum R_L and current ratio $I_{TX,1} : I_{TX,2} : I_{TX,N} = M_1 : M_2 : M_N$.

One of the two requirements for maximum efficiency tracking is the current ratio optimization between $I_{TX,k}$s [18]–[20], which is extractable, as shown in Section II-B. This optimum

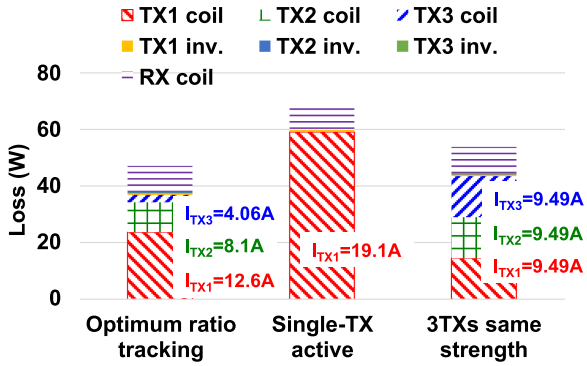

Fig. 7. Necessity of multiple-TX activation and current ratio optimization between TXs in maximum efficiency tracking. The rectifier voltage of each configuration is set to be the same.

current ratio is plotted as green solid line in Fig. 2. The maximum efficiency occurs at a certain $(I_{TX,1}, I_{TX,2})$ point on $I_{TX,1} : I_{TX,2} = 2 : 1$ line. In Fig. 7, the loss breakdown between different driving methods with coupling coefficient ratio of 3:2:1 is compared. The "Single-TX active" refers to the case where only TX#1, which has the highest coupling with receiver, is activated alone. The "Single-TX" configuration shows higher loss because the I_{TX1} becomes higher to deliver the same power.

The other requirement for maximum efficiency tracking is the R_L optimization because, as shown in Fig. 2, R_L differs for each magnitude of I_{TX} even when the ratio between I_{TX}s is optimized as in green line. Another observation from Fig. 2 is that even for a given R_L value, the efficiencies vary depending on the ratio between $I_{TX,1}$ and $I_{TX,2}$. Hence, both the R_L and current ratio must be tracked simultaneously.

Therefore, the aim of this section is to derive optimum TX currents that realize both aforementioned requirements, using the extracted couplings presented in Section II-B and II-C. The R_L that maximizes the total efficiency under the optimum TX current ratio is called as optimum load impedance, $R_{L,\mathrm{opt}}$, and is given as

$$R_{L,\mathrm{opt}} = R_{RX}\sqrt{1 + \frac{\omega^2 \sum_{k=1}^{N} M_k^2}{R_{TX} R_{RX}}} \tag{12}$$

for multiple-transmitter case ($N \geq 2$) [17]. From a voltage conversion ratio of a dc–dc converter, the optimum desired rectifier voltage that achieves (12) is derived as follows:

$$V_{\mathrm{rect,opt}} = \sqrt{\frac{\pi^2 R_{L,\mathrm{opt}} V_{\mathrm{rect}} I_{\mathrm{rect}}}{8}}. \tag{13}$$

Here, V_{rect} in right-hand side is a sensed rectifier voltage immediately before this calculation, and the $V_{\mathrm{rect,opt}}$ in left-hand side is the new target rectifier voltage for next cycle output. Then, the $I_{TX,k}$ that produces this $V_{\mathrm{rect,opt}}$ is calculated using (9)–(11) and (13) as follows:

$$I_{TX,k,\mathrm{opt}} = \frac{M_k\,(1 + R_{RX}/R_{L,\mathrm{opt}})}{\omega\,(M_1^2 + M_2^2 + , \ldots , + M_N^2)} \sqrt{2 R_{L,\mathrm{opt}} V_{\mathrm{rect}} I_{\mathrm{rect}}}. \tag{14}$$

This gives a proportionality factor between $I_{TX,k,\mathrm{opt}}$s and M_ks as

$$\frac{I_{TX,1,\mathrm{opt}}}{M_1} = \frac{I_{TX,2,\mathrm{opt}}}{M_2} =, \ldots, = \frac{I_{TX,N,\mathrm{opt}}}{M_N} = \frac{(1 + R_{RX}/R_{L,\mathrm{opt}})}{\omega\left(M_1^2 + M_2^2 +, \ldots, + M_N^2\right)} \sqrt{2R_{L,\mathrm{opt}} V_{\mathrm{rect}} I_{\mathrm{rect}}}. \tag{15}$$

In other words, once the coupling, the impedance parameters, and the rectifier outputs are identified, (14) provides the optimum required TX coil currents $I_{TX,k,\mathrm{opt}}$s.

The relationship between $V_{\mathrm{inv},k}$ and $I_{TX,k}$ is

$$V_{inv,k,\mathrm{opt}} = \frac{\pi}{4} \frac{1}{\omega C_{\mathrm{lcc}}} |\mathbf{I_{TX,k.opt}}|. \tag{16}$$

Hence, setting the $V_{\mathrm{inv},k}$ to $V_{\mathrm{inv},k,\mathrm{opt}}$ finishes one control cycle, which is summarized in Fig. 5(b).

Fig. 6(b) presents the optimum proportionality factor $I_{TX,k,\mathrm{opt}}/M_k$, which is given by (15). For each instantaneous RX position, the M_1, M_2, and M_3 are different, which, in turn, demands different $I_{TX,k,\mathrm{opt}}/M_k$ factors for each RX position. The multiplication of $I_{TX,k,\mathrm{opt}}/M_k$ and M_k produces the optimum required $I_{TX,k,\mathrm{opt}}$ current level for each position.

The maximum efficiency operation and the V_{Load} regulation are achieved simultaneously in this article. The constant V_{Load} is achieved for wide range of V_{rect} thanks to the RX dc–dc converter, which adjusts its duty cycle in response to V_{rect} variation. The acceptable input voltage range of RX dc–dc converter (i.e., V_{rect} range) is 10–150 V for a fixed V_{Load} in our setup. However, regarding maximum efficiency, to match the R_L of Fig. 5 to optimum $R_{L,\mathrm{opt}}$ of (12), there exists only one optimum V_{rect} value, $V_{\mathrm{rect,opt}}$, as shown in (13). In order to induce the optimum $V_{\mathrm{rect,opt}}$, the controller adjusts the TX coil currents based on the proposed equations (15), which satisfies not only the optimum V_{rect} and R_L but also the optimum ratio between TX coil currents. Referring to Fig. 2, maximum efficiency for multiple transmitters is obtained when R_L is optimized and TX current ratios are set to mutual inductance ratios.

Fig. 5(b) presents the overall control flowchart. For dynamic charging application, the M_1, M_2, …, M_N change as the receiver moves. The proposed method in (9) and (11) runtime monitors these values and outputs the optimum (14) instantly.

IV. Measurement

Fig. 8 presents the overall measurement setup. The dimensions of coils target the application of AGV. The coil is fabricated with litz wire, of which specification is 360 strands of 0.06 mm diameter. The number of turns of coil is five. TX and RX coils are 40 × 35 cm^2. The dc current sensors use LTC6101HV.

The target moving speed of RX is 10 km/h for logistic vehicle in warehouse and factory scenario. Fig. 8(a) presents that the TX coils are placed 30 cm apart each other. The RX moves from TX#1 to TX#3 at 10 km/h speed. The lateral position is defined as 0 cm at the center of TX#1 and 60 cm at the center of TX#3. In Fig. 8(b), at 45 cm, a sensor measures the speed from dip1 to dip5. Note that the speed measurement is not for control purpose—the sensor output is not connected to MCU and not used for control. It is just for plotting and data logging purpose in Fig. 10. In fact, the proposed control method does not require external sensors or detecting coils.

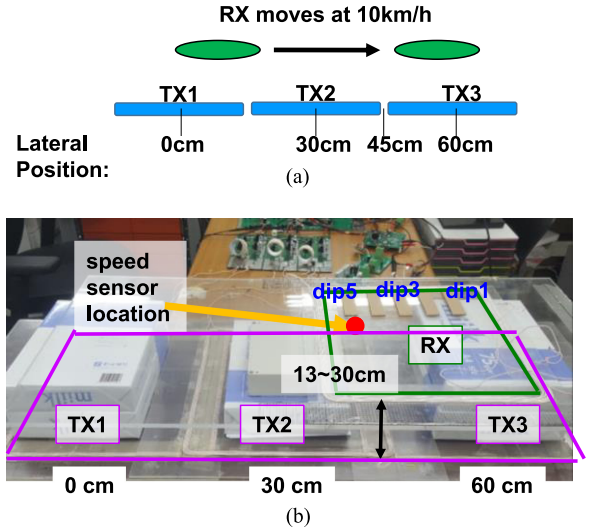

Fig. 8. Measurement setup. (a) RX moves at 10 km/h from TX1 to TX3. (b) Coil arrangements. The speed sensor is not for control purpose and not connected to MCU. It is just for data logging and plotting purpose.

TABLE I
Component Parameters

Parameter	Value	Parameter	Value
L_{TX}	32.3 μH	C_{lcc}	509.7 nF
R_{TX}	0.17 Ω	R_{lcc}	0.03 Ω
C_{TX}	92.7 nF	L_{RX}	28.2 μH
R_{RX}	0.15 Ω	P_{Load}	200 W
C_{RX}	89.8 nF	V_{Load}	35 V
TX coil size	40x35 cm	*RX coil size*	35x30 cm

Table I presents key component parameters. The derivations of Sections II–III are valid for arbitrary numbers of transmitters, whereas total three TXs are fabricated for experiment. Each inverter bridge is driven by a shared 100-kHz clock in order to make the phase and the frequency of every TX to be the same. Due to the current-source characteristic of *LCC* inverter, the phase of $\mathbf{I_{TX,k}}$ is not affected by impedance variations of coils. The three inverters are fed by a dc power supply. Total measured efficiency refers to the load power at R_{Load} divided by the total supplied power. The Cortex-A53 ARM cores in TX and RX communicate each other via WiFi, which is selected due to its low latency. The direction of data flow is from receiver to transmitter so that V_{rect} and I_{rect} information is available on TX MCU. The core also senses the voltage and current. The TX-side MCU determines and outputs the optimal $\mathbf{I_{TX}}$ currents by adjusting the $V_{\mathrm{inv},1}, \ldots, V_{\mathrm{inv},N}$ voltages. Specifically, (9), (11)–(16) are coded in the MCU. The power consumption due to MCU and communications are not included in the overall estimation of efficiency.

Fig. 9 shows the response when RX moves gradually from TX#1 to TX#3. The controller extracts instantaneous M_ks

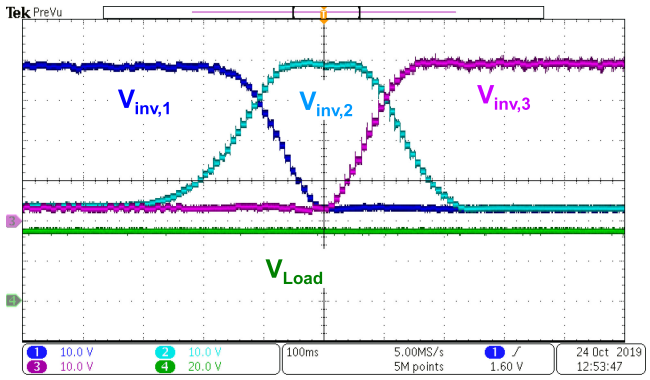

Fig. 9. RX is being moved from TX#1 to TX#3. The controller extracts instantaneous M_ks and optimizes inverter strengths for each instantaneous $M_k s$. The TXs with low coupling enter standby mode. Note that the time-domain horizontal axis of oscilloscope is not to be linearly mapped to the RX position.

and optimizes inverter strengths for each instantaneous M_ks. The TXs with low coupling enter standby mode. Due to the acceleration and deceleration of moving, the moving speed is not constant. Also, the end position of moving is not symmetric with the start position due to difficulty of RX motion mechanical control. Hence, the time-domain horizontal axis of oscilloscope is not to be linearly mapped to the RX position.

When coupling changes, the proposed method instantly extracts M_1–M_3. The optimum $R_{L,\mathrm{opt}}$ in (12) is changed due to M_1–M_3 variations, which, in turn, requires different $V_{\mathrm{rect,opt}}$ in (13). In response to that, the controller adjusts I_{TX1}–I_{TX3} in such a way that the optimum $V_{\mathrm{rect,opt}}$ is indeed developed at rectifier output. At the same time, the duty cycle of RX dc–dc converter is self-adjusted in response to varied $V_{\mathrm{rect,opt}}$ to produce a fixed V_{Load}.

Fig. 10 shows the tracking accuracy when the receiver moves at 10 km/h speed across 37–55-cm interval. Fig. 10(a) shows that $I_{TX,2}$ and $I_{TX,3}$ decreases and increases, respectively, since the 37–55-cm interval is between the boundary of TX#2 and TX#3. The measured $\mathbf{I_{TX}}$ currents during 10 km/h movement are plotted in Fig. 10(b) for each instantaneous position and compared with theoretical ideal targets. Here, the "measured" is the oscilloscope reading during 10 km/h movement. The "theoretic ideal" is manually calculated by (14) for comparison purpose. Fig. 10(c) presents the actual mutual inductance ratio, M_2:M_3, for each RX position. The $I_{TX,2}/I_{TX,3}$ ratio is the measured value during movement. From Fig. 10(b) and (c), it is clear that the system successfully extracts the instantaneous mutual inductances for each RX position and outputs optimum TX currents during runtime movement. Fig. 10(d) explains why the theoretical optimum I_{TX2} remains constant even if M_2 and M_3 change in 30–37 cm region. The optimum $I_{TX,k,\mathrm{opt}}/M_k$ value specified by (15) is the lowest at 30 cm while it gradually increases up to 45 cm (which is boundary between TX2 and TX3). However, M_2 gradually decreases from 30 to 45 cm. Note that the theoretic optimum $I_{TX,2}$ value is the multiplication of $I_{TX,k,\mathrm{opt}}/M_k$ and M_2. Hence, at 30–37 cm region, the optimum $I_{TX,2}$ value remains relatively constant although M_2 changes. Nevertheless, throughout all positions, the ratio between I_{TX2} and I_{TX3} follows the ratio of M_2 and M_3, as shown in Fig. 10(c).

While the target speed is 10 km/h, excessive moving speed may break the power delivery. Suppose that the RX is initially at 30-cm position, and hence, only $I_{TX,2}$ is activated while $I_{TX,3}$ is zero. The sensing-calculation-output period in Fig. 5(b), which is performed by a microcontroller, is ∼7 ms. During this 7-ms interval, $I_{TX,2}$ is kept high, whereas $I_{TX,3}$ is kept low. However, if the RX suddenly moves to 60-cm position (TX3 location) within this 7-ms interval, the RX cannot receive power. This is because $I_{TX,3}$ has been kept zero during this interval. In summary, if the receiver moves to standby-state TX coil within one sensing-calculation-output interval, then the power delivery fails.

Referring to Fig. 8, measurement setup, the characteristic at 30–60 cm is symmetric with that at 0–30 cm. In other words, taking the 30 cm as a center position, the characteristics at the left side and at the right side of 30 cm are the same. Therefore, the characteristic of whole range (0–60 cm) can be constructed using 30–60 cm experiment result.

Fig. 11 proves that the controller can optimize the strengths of TX coil current as well as the ratio of currents. For fixed ratio of TX currents, there exists an optimum strength of current, and the controller indeed settles to the optimum point.

Fig. 12 presents the response to load current transition from half load to full load. The controller changes V_{rect} by $\sqrt{2}$, as required by (13). The output settles in 10 ms. The glitch in I_{Load} waveform (blue trace) from 6.8 to 3.4 A transition is due to a mechanical bouncing effect of load detaching, which is a limitation of our load equipment. The sensing-calculation-output period of Fig. 5(b), which is performed by a microcontroller, is ∼7 ms. Immediately after the controller output change, it takes ∼3 ms for the power circuits to converge. Therefore, summing the two kinds of delays results in a 10-ms delay in response to load change.

Fig. 13 compares the proposed activation method (concurrent multiple-TX activation with current ratio optimization) with other activation methods. Here, "1-TX" refers to the method when only one TX is activated at a time, where the TX that has the highest coupling is chosen. The "3-TX" refers to the method that simultaneously activates all three TX coils at $I_{TX,1}$: $I_{TX,2}$: $I_{TX,3} = 1 : 1 : 1$. For all three methods, their optimum load impedances are found and set. The proposed activation with current ratio optimization achieves the highest efficiency.

For Fig. 13(b) and (c), "1-TX" activation shows low efficiency because the RX is between boundaries of two TXs and therefore weakly coupled to each TX. For such RX position, it is better to activate both TXs with current ratio optimization.

For Fig. 13(a), the RX is located at the center of TX#2. At vertical distance of 15 cm, the M_2 is much higher than M_1 and M_3. Hence, the proposed method mainly activates TX#2 only, which is similar to the "1-TX" operation. However, as the vertical separation increases, the M_2 is lowered such that M_2 becomes similar to M_1 and M_3. Therefore, TX#1, TX#2, and TX#3 are activated with similar current level to each other in the proposed method at longer vertical separation. This improves the efficiency at longer distance compared with the "1-TX" method.

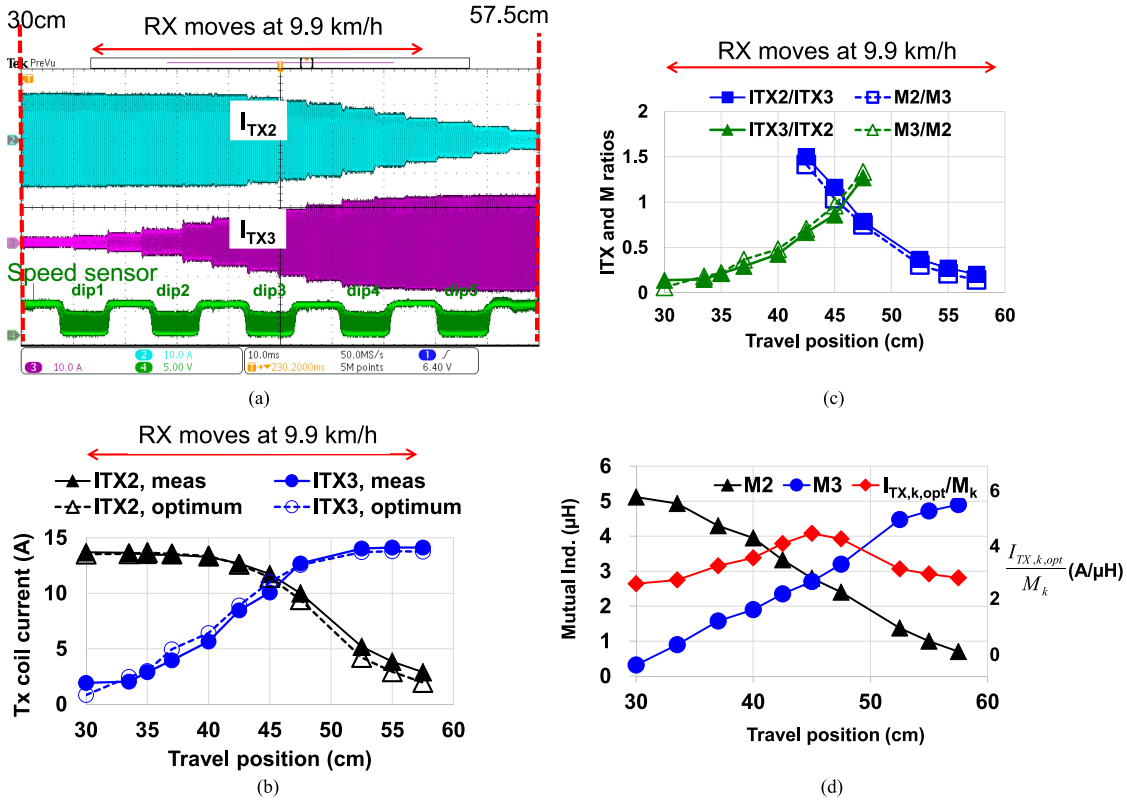

Fig. 10. For each instantaneous RX position during 10 km/h movement, the system can correctly extract the M_1–M_3 and adjust I_{TX1}–I_{TX3} accordingly. (a) I_{TX2} and I_{TX3} waveforms when the RX moves at 10 km/h speed over the 30–57.5-cm interval, which is from TX2 to TX3. (b) Measured I_{TX2} and I_{TX3} currents accurately track the target optimum value for each instantaneous RX position during 10 km/h. (c) Measured current ratio matches well with the actual mutual coupling ratio. (d) Theoretic optimum $I_{TX,k}/M_k$ ratio specified by (15). The multiplication of M_k and $I_{TX,k,\mathrm{opt}}/M_k$ gives an optimum $I_{TX,k}$ coil current, which is presented in (b).

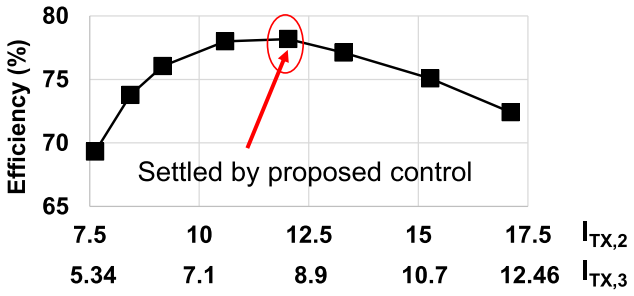

Fig. 11. Measured efficiency versus strengths of I_{TX2} and I_{TX3} while the ratio $I_{TX2}:I_{TX3}$ is kept optimum. The RX is stationary. The proposed control method successfully detects the optimum strength of $I_{TX,2}$ and $I_{TX,3}$, as well as the ratio of M_2:M_3.

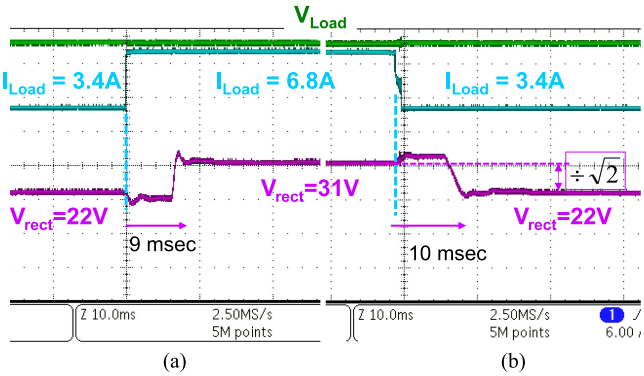

Fig. 12. Load current step change. The controller adjusts TX coil currents in such a way that V_{rect} is changed by $\sqrt{2}$ times, as required by (13). The output settles in 10 ms. (a) Load current increases. (b) Load current decreases.

Table II presents the performance comparison with prior maximum efficiency tracking techniques. The settling time of this article is only 10 ms, which is the fastest. The efficiency is low because the Q-factor of coils is lower than that presented in [9] and [11]. Fig. 14 shows that half of loss is due to the coil parasitic resistance. Similarly, the maximum theoretic efficiency of this article is lower than other works. This is because the "theoretical maximum efficiency" is a function of unloaded Q-factor of coils and coupling coefficient, as presented in [24], but the coils in our setup have low unloaded Q-factor due to high parasitic resistance. This is not a limitation of the proposed method. Moreover, in terms of power electronics circuits necessary to implement the algorithm, the proposed method does not require additional lossy semiconductor electronics because other methods such as [8], [9], and [11] also consist of TX-side

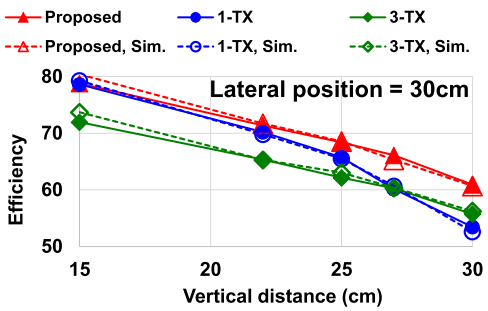

(a)

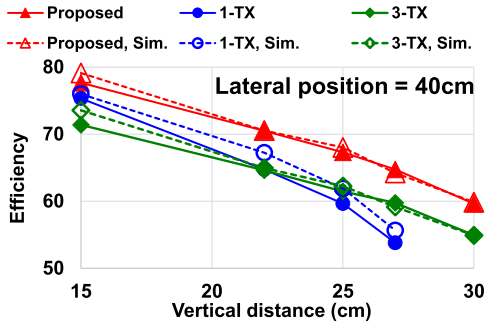

(b)

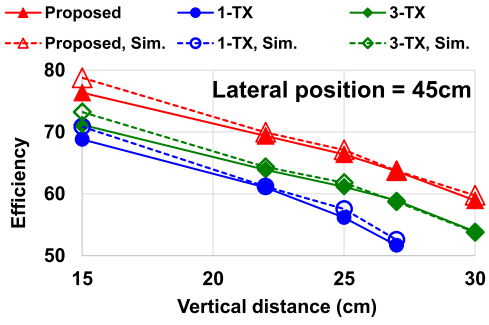

(c)

Fig. 13. Comparison with other activation methods and the proposed current ratio optimization. The proposed method achieves higher efficiency. (a) RX is at 30-cm position. (b) RX at 40 cm. (c) RX at 45 cm.

TABLE II
COMPARISON WITH PRIOR MAXIMUM EFFICIENCY TRACKING

Work	Settling Time (msec)	Number of concurrently -active TXs	Load Power (W)	Coil TX Q, RX Q	Max. Theoretic Effi. (%)	Efficiency (%)
[1]	200	1	-	-	-	n/a
[8]	120	1	10	213, 293	94.3	76
[9]	600	1	-	276, 447	94	85
[11]	300	1	90	164, 172	93	86.5
This	10	3	200	119, 118	90.3	78.8

converter, inverter, RX-side rectifier, and converter, of which structure is shared with the proposed method.

The system cost can be reduced if the magnitude of TX coil currents can be adjustable using a single inverter, which is one of future research topics. To translate to higher power

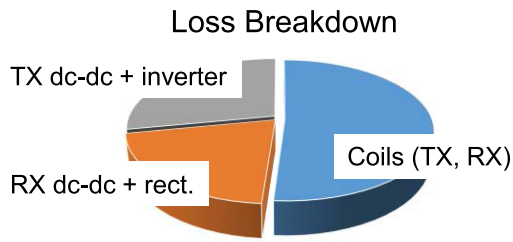

Fig. 14. Loss breakdown analysis.

level, the algorithm can be kept unmodified, but the individual power electronics designs, such as inverter and converter, and the current sensing circuitry should be improved.

V. CONCLUSION

The article develops a fast MEPT for concurrently-active multiple-transmitter array to accommodate moving receiver object. Within a sampling and update period of 7 ms, the controller senses dc voltage and current, estimates all the mutual inductances, calculates the required optimum TX coil currents, and then outputs to TX coil.

For multiple-transmitter system, it is discussed that the relative ratio between mutual inductances needs to be extracted in advance before being able to estimate the value of mutual inductances. We propose that the ratio between mutual inductances can be obtained by multiplying reflected resistances' ratio and inverter input voltages' ratio. This mutual inductance ratio along with rectifier dc quantities extracts the absolute values of M_ks.

This is the first maximum efficiency tracking that optimizes not only load impedance but also current ratios between adjacent TX coil arrays with fast response time to be suitable for dynamic charging. The tracking does not use parameter sweeping, P&O, and error integration process. The sensing requirement is easy because the control uses dc voltage and current quantities. It is demonstrated that the controller output precisely tracks the required optimum value for each instantaneous RX position during 10 km/h moving speed.

REFERENCES

[1] X. Hu, Y. Wang, Y. Jiang, W. Lei, and X. Dong, "Maximum efficiency tracking for dynamic wireless power transfer system using LCC compensation topology," in *Proc. IEEE Energy Convers. Congr. Expo.*, 2018, pp. 1992–1996.

[2] K. Takeda and T. Koseki, "Improvement of efficiency of multiple-parallel dynamic wireless power transfer system with LCC topology," in *Proc. Annu. Conf. IEEE Ind. Electron. Soc.*, 2018, pp. 4810–4815.

[3] L. Shuguang, Y. Zhenxing, and L. Wenbin, "Electric vehicle dynamic wireless charging technology based on multi-parallel primary coils," in *Proc. Int. Conf. Eng. Comput. Educ. Interactive Educ.*, 2018, pp. 120–124

[4] K. Lee, Z. Pantic, and S. Lukic, "Reflexive field containment in dynamic inductive power transfer systems," *IEEE Trans. Power Electron.*, vol. 29, no. 9, pp. 4592–4602, Sep. 2014.

[5] S. Zhou and C. Mi, "Multi-paralleled LCC reactive power compensation networks and their tuning method for electric vehicle dynamic wireless charging," *IEEE Trans. Ind. Electron.*, vol. 63, no. 10, pp. 6546–6556, Oct. 2016.

[6] Y. Liu, R. Mai, D. Liu, Y. Li, and Z. He, "Efficiency optimization for wireless dynamic charging system with overlapped DD coil arrays," *IEEE Trans. Power Electron.*, vol. 33, no. 4, pp. 2832–2846, Apr. 2018.

[7] C. Mi, G. Buja, S. Choi, and C. Rim, "Modern advances in wireless power transfer systems for roadway powered electric vehicles," *IEEE Trans. Ind. Electron.*, vol. 63, no. 10, pp. 6533–6545, Oct. 2016.
[8] D. Ahn, S. Kim, J. Moon, and I.-K. Cho, "Wireless power transfer with automatic feedback control of load resistance transformation," *IEEE Trans. Power Electron.*, vol. 31, no. 11, pp. 7876–7886, Nov. 2016.
[9] X. Dai, X. Li, Y. Li, and A. Hu, "Maximum efficiency tracking for wireless power transfer systems with dynamic coupling coefficient estimation," *IEEE Trans. Power Electron.*, vol. 33, no. 6, pp. 5005–5015, Jun. 2018.
[10] X. Tang, J. Zeng, K. P. Pun, S. Mai, C. Zhang, and Z. Wang, "Low-cost maximum efficiency tracking method for wireless power transfer systems," *IEEE Trans. Power Electron.*, vol. 33, no. 6, pp. 5317–5329, Jun. 2018.
[11] Z. Huang, S.-C. Wong, and C. Tse, "Control design for optimizing efficiency in inductive power transfer systems," *IEEE Trans. Power Electron.*, vol. 33, no. 5, pp. 4523–4534, May 2018.
[12] W. Zhong and S. Hui, "Maximum energy efficiency operation of series-series resonant wireless power transfer systems using ON-OFF keying modulation," *IEEE Trans. Power Electron.*, vol. 33, no. 4, pp. 3595–3603, Apr. 2018.
[13] H. Li, J. Fang, S. Chen, K. Wang, and Y. Tang, "Pulse density modulation for maximum efficiency point tracking of wireless power transfer systems," *IEEE Trans. Power Electron.*, vol. 33, no. 6, pp. 5492–5501, Jun. 2018.
[14] T.-D. Yeo, D. Kwon, S.-T. Khang, and J.-W. Yu, "Design of maximum efficiency tracking control scheme for closed-loop wireless power charging system employing series resonant tank," *IEEE Trans. Power Electron.*, vol. 32, no. 1, pp. 471–478, Jan. 2017.
[15] W. X. Zhong and S. Y. R. Hui, "Maximum energy efficiency tracking for wireless power transfer systems," *IEEE Trans. Power Electron.*, vol. 30, no. 7, pp. 4025–4034, Jul. 2015.
[16] M. Fu, H. Yin, X. Zhu, and C. Ma, "Analysis and tracking of optimal load in wireless power transfer systems," *IEEE Trans. Power Electron.*, vol. 30, no. 7, pp. 3952–3963, Jul. 2015.
[17] D.-H. Kim and D. Ahn, "Maximum efficiency point tracking for multiple-transmitters wireless power transfer," *IEEE Trans. Power Electron.*, to be published.
[18] S. Huh and D. Ahn, "Two-transmitter wireless power transfer with optimal activation and current selection of transmitters," *IEEE Trans. Power Electron.*, vol. 33, no. 6, pp. 4957–4967, Jun. 2018.
[19] P. K. S. Jayathurathnage, A. Alphones, D. M. Vilathgamuwa, and A. Ong, "Optimum transmitter current distribution for dynamic wireless power transfer with segmented array," *IEEE Trans. Microw. Theroy Techn.*, vol. 66, no. 1, pp. 346–356, Jan. 2018.
[20] C. Zhang, D. Lin, and S. Y. R. Hui, "Efficiency optimization method of inductive coupling wireless power transfer system with multiple transmitters and single receiver," in *Proc. IEEE Energy Covers. Congr. Expo.*, Phoenix, AZ, USA, Sep. 2016, pp. 1–6.
[21] V. Jiwariyavej, T. Imura, and Y. Hori, "Coupling coefficients estimation of wireless power transfer system via magnetic resonance coupling using information from either side of the system," *IEEE J. Emerg. Sel. Topics Power Electron.*, vol. 3, no. 1, pp. 191–200, Mar. 2015.
[22] D. Kobayashi, T. Imura, and Y. Hori, "Real-time coupling coefficient estimation and maximum efficiency control on dynamic wireless power transfer for electric vehicles," in *Proc. IEEE PELS Workshop Emerg. Technologies: Wireless Power*, 2015, pp. 1–6.
[23] A. Lusiewicz, J. Noeren, M. Jaksch, and N. Parspour, "A novel method for online coupling factor determination in inductive power transfer systems," in *Proc. IEEE Wireless Power Transf. Conf.*, 2018, pp. 1–4.
[24] M. Baker and R. Sarpeshkar, "Feedback analysis and design of RF power links for low-power bionic systems," *IEEE Trans. Biomed. Circuits Syst.*, vol. 1, no. 1, pp. 28–38, Mar. 2007.

Do-Hyeon Kim received the B.S degree from Yonsei University, Seoul, South Korea, in 2009, and the integrated master's and Ph.D. degree in power electrical equipment information and communications engineering from the University of Science and Technology, Ansan, South Korea, in 2017.

He is currently with Samsung Electronics, Suwon, South Korea. His current research interests include electromagnetic theory and wireless power transmission.

Seongmin Kim received the B.S., M.S., and Ph.D. degrees from the Department of Electronic Engineering, Kyungpook National University, Daegu, South Korea, in 1997, 1999, and 2016, respectively.

Since March 2001, he has been with the Electronics and Telecommunications Research Institute, Daejeon, South Korea. He has developed RF systems for WiFi, mobile wimax, LTE, LTE-A, and wireless power transfer (WPT). His current research interests include design and implementation of WPT system, control algorithm for WPT, and network management for WPT system.

Sang-Won Kim received the B.S. and M.S. degrees from the Department of Electronic Engineering, Sogang University, Seoul, South Korea, in 1999 and 2002, respectively.

Since 2005, he has been with the Electronics and Telecommunications Research Institute, Daejeon, South Korea. He has developed RF systems for cognitive radio, direction finding, and wireless power transfer (WPT). His research interests include RF circuit design and WPT system.

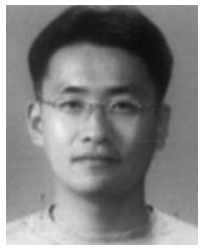

Jungick Moon received the M.S and Ph.D. degrees from the Department of Electrical Engineering, Korea Advanced Institute of Science and Technology, Daejeon, South Korea, in 2000 and 2004, respectively.

Since 2004, he has been with Electronics and Telecommunications Research Institute, as a Senior Member of Engineer Staff. His research interests include developing small antennas, broadband antennas, wireless power transmission, and RF energy harvesting.

Inkui Cho received the B.S. and M.S. degrees from the Department of Electronic Engineering, Kyungpook National University, Daegu, South Korea, in 1997 and 1999, respectively, and the Ph.D. degree in electrical engineering from Korea Advanced Institute of Science and Technology, Daejeon, South Korea, in 2007.

Since May 1999, he has been with Electronics and Telecommunications Research Institute, Daejeon, South Korea, where he has designed and developed optical backplane, optical chip-to-chip interconnect system, and magnetic resonance wireless power transfer. His current research interests include simulation and development of WPT components, such as planar magnetic resonator, magnetic resonator for three-dimensional WPT.

Dukju Ahn received the B.S. degree from Seoul National University, Seoul, South Korea, in 2007, and the M.S. and Ph.D. degrees from the Korea Advanced Institute of Science and Technology, Daejeon, South Korea, in 2010 and 2012, respectively, all in electrical engineering.

He is currently with Incheon National University, Incheon, South Korea. His research interests include wireless power transfer, power conversion, and analog/RF integrated circuit design.